9

Modelling drape deformation of woven fabrics and garments – theory

9.1 Introduction

The key to developing CAD (computer-aided design) systems for clothing products is the establishment of physically-based numerical models which can efficiently and accurately simulate the drape and other complex deformations of fabrics (Hu and Teng, 1996), in particular woven fabrics which are the commonly used fabric material. Woven fabrics are complex mechanisms made up of intersecting threads or yarns. Although they may be treated as continuous sheet materials, when undergoing overall deformations like draping, the complex and discrete microstructure and their very small thickness lend these fabrics many special properties that differ from those of other conventional sheet materials such as steel and glass. Fabrics have a very small bending stiffness compared to their membrane stiffness and have different mechanical properties in the warp and weft directions. They are easily deformable, suffering large deflections and rotations even under their own weight and in daily use. The maximum deflection involved in fabric deformations may be of the order of hundreds of times the thickness, and the final deformed shape may be extremely complicated, with many doubly-curved folds. The deformations are large although the strains are generally small. Analysis of complex fabric deformations is therefore a difficult task and one that was impossible, except for a few very simple cases, before the computer era.

Over the last two decades computer technology has made great advances. These advances have made it possible to model complex fabric deformations such as fabric draping using computer simulation techniques. There have been many successes and considerable progress in this area during the period (Hu and Teng, 1996; Ng and Grimsdale, 1996). Most early works (Weil, 1986; Dhande *et al.*, 1993) in the area are geometrically based, with an emphasis on reproducing the cloth-like appearance of a fabric sheet on a computer. These models cannot simulate fabric behaviour physically since no mechanical properties are included in them. Many other workers,

however, have adopted various physically-based models (Hu and Teng, 1996).

Feynman (1986) proposed an energy-based physical model for simulating the appearance of cloth. The simulations included hanging cloth and cloth draped over a sphere. The total energy function of the model contains tensile strain, bending strain and gravity terms, but shear deformations are not considered. Terzopoulos *et al.* (1987) introduced an elastically deformable model for generalised flexible objects including fabrics. Since the model was developed for general use in computer graphics, it is not capable of directly incorporating standard engineering parameters such as Young's modulus. The solution procedure for the equations arising from the model is also computationally intensive. Many other works (Thalmann and Yang, 1991; Thalmann and Thalmann, 1991; Carignan *et al.*, 1992) were reported using and extending Terzopoulos *et al.*'s deformable model. These works were focused on the computer visualisation and animation of garments.

Breen *et al.* developed a particle-based model to simulate the draping behaviour of woven cloth (Breen 1993; Breen *et al*. 1991, 1992, 1994). In their model, the cloth is treated as a collection of particles that conceptually represent the crossing points of warp and weft threads in a plain-woven fabric. Separate empirical energy functions were proposed for yarn repelling, stretching, bending and trellising deformations. These functions were tuned using the KES, Kawabata Evaluation System (Kawabata, 1975), test data empirically in their later works (Breen *et al.*, 1992; Breen, 1993). The final position of the draped fabric was determined based on the minimisation of the total potential energy which is the sum of the deformation energy terms mentioned above and the potential energy of the self weight. While the model was conceptually based on the microstructure of cloth, continuum-based macrostructure properties were used in the simulation. The particle grid of 51×51 used for a 1 m $\times$ 1 m cloth in the numerical examples is also far from that necessary for a microstructural or thread level model. In addition, the solution procedure employing a stochastic searching process was reported to be very time-consuming. Recently Eberhardt *et al.* (1996) extended Breen's particle-based model by using a different, faster technique to compute the exact particle trajectories. Some promising simulations including cloth draped over a square table, a circular table and a sphere were presented.

Stylios *et al.* (1995, 1996) presented a physically-based approach using the deformable node-bar model (Schnobrich and Pecknold, 1973) to predict complex deformations of fabrics. In their approach, the fabric sheet is assumed to be a continuum shell with homogeneous, orthotropic and linearly elastic properties. Their drape simulation was compared with results from a fabric drape testing system. The modelling of a skirt attached to a synthetic lady was also described.

Several other researchers employed the finite-element method for the simulation of fabric draping behaviour. Lloyd (1980) was probably the first to apply the finite-element method to model fabrics and dealt only with in-plane deformations. Collier (1991) developed a large deflection/small strain analysis employing a 4-noded orthotropic flat shell element to predict the drape coefficient of cotton fabrics. Their results were reported to be in reasonably good agreement with experimental results. Gan *et al.* (1995) produced a similar analysis employing a curved shell element and presented simulation results for fabric sheets draped over square and circular pedestals. Kim (1991) described drape simulations using a geometrically exact shell theory proposed by Simo *et al.* (1989, 1990). Simo and Fox (1989), Deng (1994) and Eischen *et al.* (1996) extended the work of Kim to buckling, contact and materially non-linear problems.

Chen and Govindaraj (1995) predicted the draping of fabrics using a shear flexible shell theory. The predicted results of a square fabric sheet draped over a flat square surface and an animation sequence were presented. Yu *et al.*(1993) and Kang and Yu (1995) also developed a non-linear finite-element code to simulate the draping of woven fabrics. In their study, a flat shell element model based on a convected co-ordinate system (Simo and Fox, 1989; Simo *et al.*, 1989, 1990; Bathe, 1982) was used. The fabric was again assumed to be an elastic and orthotropic material. The predicted draped shapes were shown to agree reasonably well with those obtained experimentally.

Ascough *et al.* (1996) adopted a rather simple beam element model in their cloth drape simulations and the simulation results for a piece of fabric draped over a table corner do not appear to be close in shape to that seen in a corresponding photo. They also presented simulation results of the falling of a skirt from its initial position into contact with a human body. Their simulations were carried out as a dynamic analysis using Newmark's method.

As reviewed above, there exist basically two main approaches in the existing modelling approaches of fabric drape deformations: (a) the finite-element approach employing a shell element; (b) a more empirical approach developed specifically for fabric deformation analysis, among which the particle-based model of Breen *et al.* is representative and the most widely quoted (Breen 1993; Breen *et al.* 1991, 1992, 1994).

The studies of Stylios *et al.* (1995; 1996) and Ascough *et al.* (1996) do not fall neatly into either of the above two approaches, but both are closely related to the first approach.

The finite-element approach employing a shell element has been used by a number of researchers. It has a rigorous mechanical basis and can be easily understood and further developed by the computational mechanics community. As the method was not developed making use of the special characteristics of fabric drape deformations, it has a number of disadvantages. First, the method entails a high computational cost as high-order shape functions are

used and very large displacements have to be followed in a step-by-step manner. Second, when the popular degenerated shell elements are used, the bending stiffness and the membrane stiffness of the shell surface will be coupled, and this subsequently leads to difficulty in modelling fabric sheets due to their independent membrane and bending stiffness. Thirdly, the method is theoretically complex, making it more difficult to be readily accepted and understood by its users.

On the other hand, the widely cited particle-based model of Breen and its extension (Breen *et al*., 1991, 1992; Breen, 1993; Breen *et al.*, 1994; Eberhardt *et al.*, 1996) contains much empiricism in the establishment of the energy functions and uses definitions of deformations which do not follow a rigorous mechanics approach. The computational cost may also be very high.

9.2 Finite-volume formulation

9.2.1 Discretisation scheme

Fabric drape deformations involve very large deflections, but the associated strains are small. This is because fabric sheets are very thin and flexible, so most of the gross deformations come from bending; the amount of in-plane stretching is very small in comparison. This means that an initial patch of a fabric sheet would retain its original surface area and volume after drape deformations.

Based on this knowledge, the finite-volume method is adopted for simulating the complex deformations of fabrics. In this method, an initially flat fabric is first subdivided into a finite number of structured small patches finite volumes (or control volumes). One control volume contains one grid node. The deformations of a typical volume can be defined using the global co-ordinates of its grid node and several neighbouring grid nodes surrounding it. The strains and curvatures, and hence the in-plane membrane and out-of-plane bending strain energies, of the whole fabric sheet are then calculated very easily over all control volumes which retain their original surface areas and thicknesses. The equilibrium equations of the fabric sheet are derived employing the principle of stationary total potential energy. Geometric non-linearity and linear elastic orthotropic material properties of the fabric are considered in the formulation. This leads to a simple but rigorous way of formulating the equilibrium equations of a grossly deformed fabric sheet.

The concept of finite volume or control volume was originally used for the discretisation of differential equations, particularly in computational fluid dynamics (Patankar, 1980; Versteeg and Malalasekera, 1995). Using this discretisation approach, the calculation domain is first divided into many non-overlapping control volumes such that there is one volume surrounding each grid node. The differential equations are then integrated over each control volume, resulting in discretisation equations containing variables for

a group of grid nodes. The most attractive feature of the finite-volume formulation is that the integral conservation of physical quantities such as mass, momentum, and energy is exactly satisfied over any group of control volumes (including the limiting case of a single finite volume) and, of course, over the whole calculation domain (Patankar, 1980).

In recent years, the finite-volume method has also been applied to solid and structural mechanics problems (Fryer *et al*., 1991; Demirdzic and Martinovic, 1993; Demirdzic and Muzaferija, 1994; Onate *et al*., 1994; Bailey and Cross, 1995; Wheel, 1996, 1997), particularly for solid body stress analysis (Demirdzic and Martinovic, 1993; Demirdzic and Muzaferija, 1994; Onate *et al*., 1994; Bailey and Cross, 1995; Wheel, 1996).

Here we attempt to extend the finite-volume method to model fabric deformation, a highly non-linear problem of orthotropic sheet materials with unique features. The deformations and energies are calculated over all control volumes based on simple but reasonable assumptions. The discretised equations containing the global co-ordinates of grid nodes as unknowns are derived using the principle of stationary total potential energy. The proposed formulation gives the finite-volume method an explicit physical interpretation in fabric deformation modelling and extends the horizon for the application of the finite-volume method.

There is another major difference between the analysis of fabric drape deformation and a non-linear load-resisting structure. In fabric deformation analysis, attention is given to the final shape of the deformed fabric sheet under self weight with or without additional applied load, while in the analysis of a non-linear load-bearing structure, the maximum load that the structure can carry and the load-deflection response are of more interest. In addition, both the displacements and the internal forces need to be carefully determined in the analysis of load-bearing structures while, in fabric deformation analysis, the final displacements are the only focus. These aspects are exploited here in developing an efficient solution method.

9.2.2 Finite-volume discretisation

Before deformations, the fabric sheet is assumed to be flat. The whole fabric surface is taken to be the computational domain of the problem, over which an appropriate discretisation grid needs to be established.

9.2.2.1 General control-volume discretisation

Consider an initially flat fabric sheet, which consists of two orthogonal sets of threads, warp and weft yarns. Figure 9.1 illustrates the domain discretisation scheme of such a fabric sheet. The dashed lines in the two orthogonal directions (warp and weft or x- and y-) divide the whole fabric area into a finite number

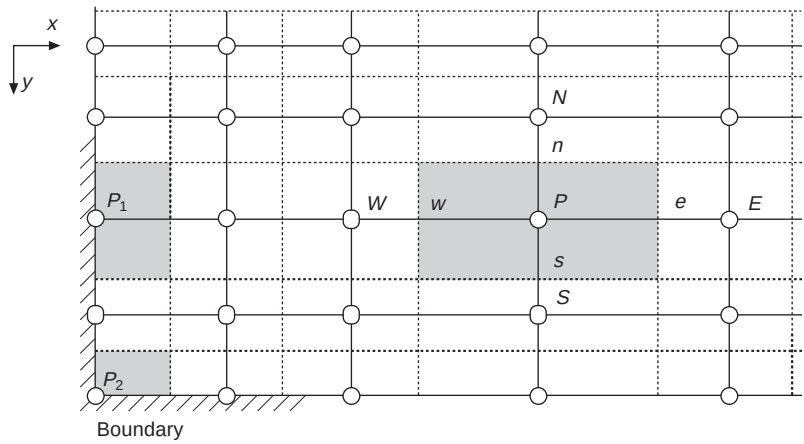

9.1 Two-dimensional non-uniform grid.

of structured sub-domains, called finite volumes (or control volumes). The solid lines are located midway between neighbouring dashed lines. Consequently, the crossings of solid lines, which are called grid nodes, lie exactly at the geometric centres of the control volumes, while the crossings of dashed lines and solid lines, which are called face nodes, lie at the mid-points of the respective finite-volume boundaries or faces.

A system of notation for each control volume is now established as shown in Fig. 9.1 for a typical internal volume. It contains one grid node which is identified by *P* and four face nodes which are identified by *w*, *e*, *n* and *s*, denoting the west, east, north and south side faces, respectively. The same letter *P* is also used to identify this typical volume. Four neighbouring grid nodes, identified by *W*, *E*, *N* and *S* respectively, are connected directly with the node *P*. Here nodes *W* and *E* are *x* direction neighbours of *P*, while *N* and *S* are the *y* direction neighbours. The two axes are assumed to be aligned with the two orthogonal directions of a woven fabric composed of warp and weft yarns. For simplicity of presentation here, the *x*-axis is assumed to be in the warp direction and the *y*-axis to be in the weft direction.

If the grid intervals (or finite-volume sizes) are non-uniform, the four face nodes will not lie midway between the grid node *P* and its four neighbouring grid nodes *W*, *E*, *N* and *S*, respectively. The positions of the four face nodes are, however, simply determined by a linear interpolation between the adjacent grid nodes. In particular, if a two-dimensional fabric drape problem is considered, the initial grid will be one-dimensional. This discretisation scheme is given in Fig. 9.2.

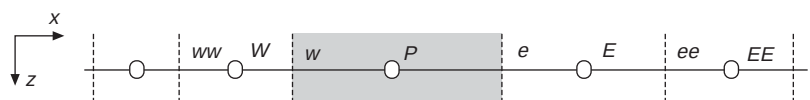

9.2 One-dimensional grid.

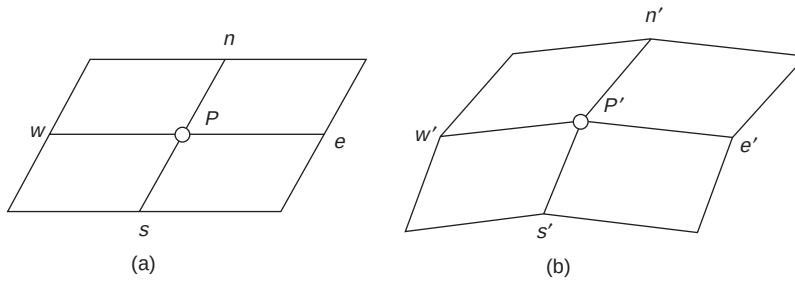

9.3 A typical control volume *P:* (a) before and (b) after deformation.

9.2.2.2 Assumptions about deformation

Deformation will lead to a subsequent change in the location and the overall shape of each control volume. For a typical control volume *P* (Fig. 9.3), this means that the grid node *P* and the face nodes *w*, *e*, *n* and *s* will move from their initial positions to their new positions. Since the fabric undergoes large displacements and rotations but small strains during the process of deformations, it may be reasonable to make the following assumptions in the analysis of fabric deformations:

(1) The fabric is an elastic and orthotropic material whose two principal directions of anisotropy coincide with the warp and weft directions of the yarns, respectively. Although the displacements may be very large, considering the small strains involved, the two directions of the warp and weft yarns are assumed to remain orthogonal throughout the deformation process.
(2) For a typical control volume, only uncoupled out-of-plane bending and in-plane tension or compression and shearing are produced during the deformation process. The contribution of twisting deformation to the strain energy is ignored.
(3) The surface area and thickness of the fabric sheet, and hence those of a control volume, do not change significantly during deformations.
(4) The strains and curvatures of a typical control volume can be determined using the positions of its grid node and four face nodes.
(5) The deformed position of each face node can be determined using a linear interpolation between its two adjacent grid nodes as in the undeformed state. For example, the deformed position of the face node *e* in Fig. 9.1 can be found by linear interpolation of the deformed positions of nodes *P* and *E*.
(6) Each grid node has three degrees of freedom: three global coordinates *x*, *y* and *z*.

Under the above assumptions, the deformations of an internal control volume will only depend on five grid nodes: the grid node of the volume itself and its four neighbours surrounding it.

In assumption 2, the twisting shear strain energy is assumed to be negligible. This assumption in fact has been involved in all fabric deformation models based on approach b, although it has never been discussed or even mentioned in these studies. Physically, the assumption may be justified by noting that the warp and weft yarns of a woven fabric structure can slide against each other under twisting shear stresses, a situation which also makes the in-plane shear stiffness much smaller than the tensile stiffness. The assumption of ignoring the resistance offered by twisting shear deformations is also supported by numerical comparisons later (Press *et al.*, 1992).

9.2.2.3 Boundary control volumes

So far, no discussion has been given on the control volumes that lie along the edges or at the corners of the computational domain. Since boundary conditions are usually imposed only on the grid nodes, the solid grid lines are placed along the domain edges, leading to half volumes along edges and quarter volumes at corners. That is, the typical edge volume P_1 (Fig. 9.1) may be viewed as a 'half' of an internal control volume and the corner volume P_2 (Fig. 9.1) a 'quarter' of an internal volume. Therefore, the deformations of the edge control volume P_1 will depend on four grid nodes instead of five, one of itself and three neighbours, and those of the corner control volume P_2 depend only on three grid nodes.

9.2.3 Strain energy

The out-of-plane bending and in-plane membrane strain energies of a typical control volume are considered in this section. The total strain energy of a control volume is the summation of these two types of strain energy. The total strain energy of the fabric sheet can be found by adding together the contributions from all control volumes.

9.2.3.1 Out-of-plane bending

The bending deformations of a typical control volume P are in general produced simultaneously in two directions: warp (or x) and weft (or y). Figure 9.4a illustrates the x-direction bending. Although the draped shape of a fabric sheet is in general a complicated curved surface, the radii of curvature in both the warp and weft directions of a small surface area are still much greater than its thickness. Therefore, if the control volume is sufficiently small, it is not difficult to derive the equivalent bending curvatures in the

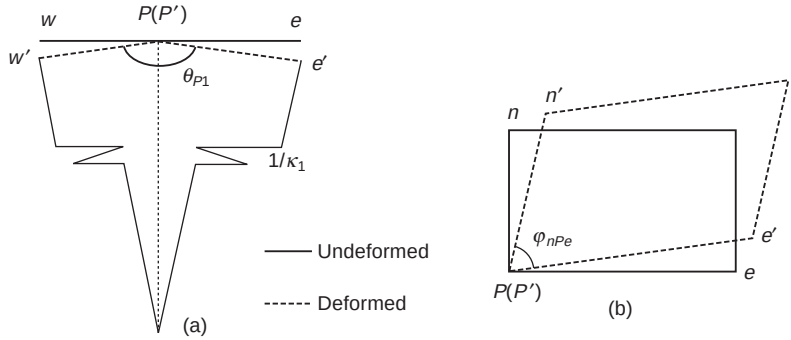

9.4 Deformations of a typical control volume *P:* (a) out-of plane bending in *x*-direction; (b) in-plane tension and shearing.

two directions from the two bending angles formed by its grid node and the four neighbours. For example, the radius of curvature of the deformed surface in the warp direction is found as the radius of a circular arc which has two end tangents coinciding with the deformed lines $P'w'$ and $P'e'$ for the control volume P (Fig. 9.4a). Therefore, the curvatures of the control volume P in the two directions are

$$\kappa_{P1} = 2\text{ctg}\,\frac{\theta_{P1}}{2}/l_{P1} \quad \text{and} \quad \kappa_{P2} = 2\text{ctg}\,\frac{\theta_{P2}}{2}/l_{P2} \qquad [9.1]$$

where κ_{P1} and κ_{P2} are the bending curvatures in the warp and weft directions, θ_{P1} and θ_{P2} are the corresponding bending angles (see Fig. 9.4a), l_{P1} and l_{P2} are the finite-volume sizes in the two directions, respectively. Based on assumptions 1–6 as given in the previous section, the bending strain energy is given as

$$U_{Pb} = \frac{1}{2}(D_1\kappa_{P1}^2 + 2D_{12}\kappa_{P1}\kappa_{P2} + D_2\kappa_{P2}^2) \cdot A_P \qquad [9.2]$$

where D_1 and D_2 are the bending rigidities in the warp and weft directions, respectively, D_{12} is the bending rigidity reflecting the Poisson's effect, and A_P is the in-plane surface area of volume P which is assumed to remain constant during deformations.

Based on the classical continuum bending theory which assumes that the tensile and compressive Young's moduli are the same and that they are also the same regardless of the nature of deformations, these bending rigidities can be related to the elastic moduli obtained from uniaxial tensile tests. For a woven fabric, however, the situation is quite different in that the measured bending rigidities are much smaller than those calculated using the conventional continuum mechanics approach. That is, a fabric has independent bending stiffness and stretching stiffness. Therefore, equation 9.2 is used directly with measured bending rigidities.

9.2.3.2 In-plane tension and shearing

The in-plane (or membrane) deformations of a control volume include tension/compression in the two principal directions and membrane shearing. In general, the surface of a control volume is not plane after deformations, so subdivision of the volume into smaller sections is desirable for a more accurate evaluation of the in-plane strain energy. Referring to the typical volume *P* as shown in Figs 9.1 and 9.3, the two lines *ew* and *ns* subdivide the whole volume into four sections, *nPe*, *nPw*, *sPe* and *sPw*. The in-plane deformations of the quarter section *nPe* are illustrated in Fig. 9.4b. The membrane strains of the section can then be evaluated as

$$\left.\begin{aligned}
\varepsilon_1 &= \varepsilon_{Pe} = \frac{\overline{P'e'} - \overline{Pe}}{\overline{Pe}} = \frac{\overline{P'E'} - \overline{PE}}{\overline{PE}} = \frac{d_{PE} - l_{PE}}{l_{PE}} \\
\varepsilon_2 &= \varepsilon_{Pn} = \frac{\overline{P'n'} - \overline{Pn}}{\overline{Pn}} = \frac{\overline{P'N'} - \overline{PN}}{\overline{PN}} = \frac{d_{PN} - l_{PN}}{l_{PN}} \\
\varepsilon_{12} &= \gamma_{nPe} = \frac{\pi}{2} - \varphi_{nPe}
\end{aligned}\right\} \qquad [9.3]$$

where l_{PE}, d_{PE} and l_{PN}, d_{PN} are the distances between grid nodes *P* and *E*, and *P* and *N*, before and after deformations, respectively; φ_{nPe} is the angle formed by lines *Pe* and *Pn* after deformations (Fig. 9.4b).

As the fabric is assumed to be an orthotropic elastic material, the corresponding stress resultants (force per unit length) in the section can be easily obtained as

$$\begin{Bmatrix} N_1 \\ N_2 \\ S_{12} \end{Bmatrix} = \begin{bmatrix} E_1 & E_{12} & 0 \\ E_{12} & E_2 & 0 \\ 0 & 0 & G \end{bmatrix} \begin{Bmatrix} \varepsilon_1 \\ \varepsilon_2 \\ \gamma_{12} \end{Bmatrix} = \begin{bmatrix} E_1 & E_{12} & 0 \\ E_{12} & E_2 & 0 \\ 0 & 0 & G \end{bmatrix} \begin{Bmatrix} \varepsilon_{Pe} \\ \varepsilon_{Pn} \\ \gamma_{nPe} \end{Bmatrix} \qquad [9.4]$$

where *G* is the shear rigidity and E_1, E_2, E_{12} are given by

$$\left.\begin{aligned}
E_1 &= \frac{E_{\text{warp}}}{1 - \nu_{\text{warp}}\nu_{\text{weft}}} \\
E_2 &= \frac{E_{\text{weft}}}{1 - \nu_{\text{warp}}\nu_{\text{weft}}} \\
E_{12} &= \frac{\nu_{\text{warp}} E_{\text{weft}}}{1 - \nu_{\text{warp}}\nu_{\text{weft}}} = \frac{\nu_{\text{weft}} E_{\text{warp}}}{1 - \nu_{\text{warp}}\nu_{\text{weft}}}
\end{aligned}\right\} \qquad [9.5]$$

Here, E_{warp} and E_{weft} are the membrane rigidities of the fabric sheet in the warp and weft directions respectively determined from tensile tests, and ν_{warp} and ν_{weft} are the corresponding Poisson's ratios. The in-plane strain energy of section *nPe* is therefore given by

$$U_{nPe} = \frac{1}{2}(E_1\varepsilon_{Pe}^2 + 2E_{12}\varepsilon_{Pe}\varepsilon_{Pn} + E_2\varepsilon_{Pn}^2 + G\gamma_{nPe}^2) \cdot A_{nPe} \qquad [9.6]$$

where A_{nPe} is the area of quarter section *nPe*.

The in-plane strain energy U_{nPw}, U_{sPw} and U_{sPe} of the other three quarter sections can be found in a similar manner. The in-plane (or membrane) strain energy of the whole control volume is the sum of the above four sections given by

$$U_{P\mathrm{m}} = U_{nPe} + U_{nPw} + U_{sPw} + U_{sPe} \qquad [9.7]$$

The total strain energy of the control volume P is the sum of bending and membrane strain energies, i.e.

$$U_P = U_{P\mathrm{b}} + U_{P\mathrm{m}} \qquad [9.8]$$

Consequently, the total strain energy of the whole fabric sheet consisting of r control volumes U_{df} is

$$U_{df} = \sum_{P=1}^{r} U_P \qquad [9.9]$$

9.2.4 Governing equations

Under its own weight and given boundary conditions, a fabric sheet always deforms into a final stable equilibrium state and forms a complicated surface, the process of which is called fabric draping. Complex deformations may also occur under additional applied loads. The final equilibrium state of the fabric can be determined by using the principle of stationary total potential energy. The total potential energy Π is the summation of the total strain energy as given by equation 9.9 and the potential energy of gravitational forces and other applied loads

$$\left.\begin{aligned} \Pi &= U_{df} + U_{\mathrm{g}} + U_{\mathrm{ex}} = \sum_{P=1}^{n}(U_{P\mathrm{b}} + U_{P\mathrm{m}} + U_{P\mathrm{g}} + U_{P\mathrm{ex}}) \\ U_{P\mathrm{g}} &= -m_P g z_P \end{aligned}\right\} \qquad [9.10]$$

where U_{g} and U_{ex} are the potential energies of gravitational forces and other applied loads respectively, m_P is the mass of the finite volume P, g is the gravitational acceleration, and z_P is the vertical co-ordinate. The equilibrium equations can be obtained using the variational principle that the total potential energy Π must be stationary;

$$\delta\Pi = \delta(U_{df} + U_{\mathrm{g}} + U_{\mathrm{ex}}) = 0 \qquad [9.11]$$

or

$$\frac{\partial\Pi}{\partial x_{Pi}} = \frac{\partial U_{df}}{\partial x_{Pi}} + \frac{\partial(U_{\mathrm{g}} + U_{\mathrm{ex}})}{\partial x_{Pi}} = 0 \quad (P = 1, 2, \ldots, r, i = 1, 2, 3) \qquad [9.12]$$

where x_{Pi} ($i = 1, 2, 3$) stands for the three global co-ordinates x_P, y_P and z_P of the position of node P at any point of time during deformation. Equation 9.12 leads to a set of non-linear algebraic equations with the global coordinates of all grid nodes as unknowns, which can be cast in the following form

$$\left.\begin{aligned} \boldsymbol{F} - \boldsymbol{R} &= 0 \\ \boldsymbol{F} &= \frac{\partial U_{df}}{\partial \boldsymbol{X}} \\ \boldsymbol{R} &= -\frac{\partial (U_{\mathrm{g}} + U_{\mathrm{ex}})}{\partial \boldsymbol{X}} \end{aligned}\right\} \qquad [9.13]$$

where $\boldsymbol{X} = [\cdots x_{W1}\ x_{W2}\ x_{W3}\ \cdots x_{P1}\ x_{P2}\ x_{P3}\ \cdots]^{\mathrm{T}}$ is the global nodal co-ordinate vector, $\boldsymbol{F}$ is the global nodal internal force vector and $\boldsymbol{R}$ is the global nodal load vector due to gravity and applied loads.

Using the Newton–Raphson iteration scheme (Bathe, 1996; Crisfield, 1991), equation 9.13 can be rewritten in the following iterative form

$$\left.\begin{aligned} \boldsymbol{K}\Delta\boldsymbol{X} &= \boldsymbol{R} - \boldsymbol{F} \\ \boldsymbol{X}^{(i+1)} &= \boldsymbol{X}^{(i)} + \Delta\boldsymbol{X} \\ \boldsymbol{K} &= \frac{\partial \boldsymbol{E}}{\partial \boldsymbol{X}} = \frac{\partial^2 U_{df}}{\partial \boldsymbol{X}\partial \boldsymbol{X}} \end{aligned}\right\} \qquad [9.14]$$

where $\boldsymbol{K}$ is the global tangent stiffness matrix of the fabric sheet, and $\boldsymbol{X}^{\{i\}}$ denotes the i-th iterative solution of the vector $\boldsymbol{X}$. From equation 9.9, the global internal force vector and the global tangent stiffness matrix may be written in the form of summations as

$$\left.\begin{aligned} \boldsymbol{F} &= \sum_{P=1}^{r} \frac{\partial U_p}{\partial \boldsymbol{X}} \\ \boldsymbol{K} &= \sum_{P=1}^{r} \frac{\partial^2 U_p}{\partial \boldsymbol{X}\partial \boldsymbol{X}} \end{aligned}\right\} \qquad [9.15]$$

Since the strain energy function U_P depends only on the co-ordinates of node P and its four neighbours W, E, N and S, only 15 components in the vector $\partial U_P/\partial \boldsymbol{X}$ are non-zero. Similarly, the matrix $\partial^2 U_P/\partial \boldsymbol{X}\partial \boldsymbol{X}$ contains only 15×15 non-zero elements. These non-zero elements form a sub-vector $\boldsymbol{F}^{\mathrm{e}}$ and a sub-matrix $\boldsymbol{K}^{\mathrm{e}}$, which are referred to as the element internal force vector and the element tangent stiffness matrix, respectively. Once all the element vectors $\boldsymbol{F}^{\mathrm{e}}$ and matrices $\boldsymbol{K}^{\mathrm{e}}$ are obtained, they can be assembled to form the global vector $\boldsymbol{F}$ and matrix $\boldsymbol{K}$, the procedure of which is similar to that in the finite-element method.

9.2.4.1 The element internal force vector

In this section, the internal force vector for a typical internal control volume P (referred to as element internal force vector here) is formulated. The vector is given by

$$\boldsymbol{F}^{\mathrm{e}} = \left[\frac{\partial U_P}{\partial x_{Wi}} \; \frac{\partial U_P}{\partial x_{Ni}} \; \frac{\partial U_P}{\partial x_{Pi}} \; \frac{\partial U_P}{\partial x_{Si}} \; \frac{\partial U_P}{\partial x_{Ei}} \right]^{\mathrm{T}} \qquad [9.16\}$$

and the corresponding element nodal co-ordinate vector is

$$\boldsymbol{X}^{\mathrm{e}} = [x_{Wi} \quad x_{Ni} \quad x_{Pi} \quad x_{Si} \quad x_{Ei}]^{\mathrm{T}} \qquad [9.17]$$

In equations 9.16 and 9.17, each component denotes a 3×1 vector, for example

$$\left\{ \frac{\partial U_P}{\partial x_{P_i}} \right\} = \left[\frac{\partial U_P}{\partial x_{P1}} \quad \frac{\partial U_P}{\partial x_{P2}} \; \frac{\partial U_P}{\partial x_{P3}} \right]^{\mathrm{T}} \quad \text{and} \quad \{x_{Pi}\} = [x_{P1} \quad x_{P2} \quad x_{P3}]^{\mathrm{T}} \qquad [9.18]$$

From equations 9.7 and 9.8, it is easy to see that

$$\left.\begin{aligned} \frac{\partial U_P}{\partial x_j} &= \frac{\partial U_{P\mathrm{b}}}{\partial x_j} + \frac{\partial U_{P\mathrm{m}}}{\partial x_j} \\ \frac{\partial U_{P\mathrm{m}}}{\partial x_j} &= \frac{\partial U_{nPw}}{\partial x_j} + \frac{\partial U_{nPe}}{\partial x_j} + \frac{\partial U_{sPw}}{\partial x_j} + \frac{\partial U_{wPe}}{\partial x_j} \\ (x_j &= x_{Wi}, x_{Ni}, x_{Pi}, x_{Si}, x_{Ei}, i = 1, 2, 3) \end{aligned}\right\} \qquad [9.19]$$

Noting that

$$\left.\begin{aligned} \kappa_{P1} &= \frac{2}{l_{P1}} \operatorname{ctg} \frac{\theta_{P1}}{2} = \pm \frac{2}{l_{P1}} \sqrt{\frac{1 + \cos\theta_{P1}}{1 - \cos\theta_{P1}}} = \pm \frac{2}{l_{P1}} \sqrt{\frac{1 + f_{wpe}}{1 - f_{wpe}}} \\ \kappa_{P2} &= \frac{2}{l_{P2}} \operatorname{ctg} \frac{\theta_{P2}}{2} = \pm \frac{2}{l_{P2}} \sqrt{\frac{1 + f_{nps}}{1 - f_{nps}}} \end{aligned}\right\} \qquad [9.20]$$

where f_{wPe} and f_{nPs} denote the cosines of the bending angles θ_{P1} and θ_{P2} respectively, the strain energies $U_{P\mathrm{b}}$, U_{nPw}, U_{nPe}, U_{sPw} and U_{wPe} can be expressed as functions of the nodal co-ordinates, that is

$$
\begin{aligned}
U_{Pb} &= \frac{1}{2}(D_1\kappa_{P1}^2 + 2D_{12}\kappa_{P1}\kappa_{P2} + D_2\kappa_{P2}^2)A_P \\
&= \frac{2D_1 l_{P2}}{l_{P1}}\frac{1+f_{wPe}}{1-f_{wPe}} \\
&\quad \pm 4D_{12}\sqrt{\frac{1+f_{wPe}}{1-f_{wPe}}\cdot\frac{1+f_{nPs}}{1-f_{nPs}}} + \frac{2D_2 l_{P1}}{l_{P2}}\frac{1+f_{nPs}}{1-f_{nPs}}
\end{aligned}
\qquad [9.21]
$$

and

$$
\left.
\begin{aligned}
U_{bPa} &= \frac{1}{2}(E_1\varepsilon_{Pa}^2 + 2E_{12}\varepsilon_{Pa}\varepsilon_{Pb} + E_2\varepsilon_{Pb}^2 + G\gamma_{bPa}^2)A_{bPa} \\
\gamma_{bPa} &= \frac{\pi}{2} - \arccos f_{bPa} \\
\varepsilon_{Pa} &= \frac{d_{PA} - l_{PA}}{l_{PA}} \quad (Pa = Pw, Pe, Pn, Ps;\ PA = PW, PE, PN, PS) \\
(bPa &= nPw, nPe, sPw, sPe)
\end{aligned}
\right\}
\qquad [9.22]
$$

where

$$
\left.
\begin{aligned}
f_{bPa} &= \frac{h_{bPa}}{g_{bPa}} \\
h_{bPa} &= \sum_{j=1}^{3}[(x_{Bj} - x_{Pj})(x_{Aj} - x_{Pj})] \\
g_{bPa} &= d_{PA}d_{PB} \\
d_{PA} &= \sqrt{\sum_{j=1}^{3}(x_{Aj} - x_{Pj})^2}\,,\ d_{PB} \\
&= \sqrt{\sum_{j=1}^{3}(x_{Bj} - x_{Pj})^2}\ (A, B = W, E, N, S) \\
(bPa &= wPe, nPs, \mathbf{nPw}, nPe, sPw, sPe)
\end{aligned}
\right\}
\qquad [9.23]
$$

where f_{bPa} denotes the cosine of the angle formed by grid lines PA and PB after deformations ($A, B = W, E, N$ or S), while d_{PA} and d_{PB} are the distances between grid nodes P and A, and P and B, respectively, after deformations. In equation 9.21 above, if the control volume deforms into an anticlastic surface, the second term on the right-hand side assumes the negative sign and otherwise the positive sign. Using equations 9.21–9.23, the first partial derivatives of the bending and membrane strain energy functions, namely the components of the element internal force vector $\boldsymbol{F}^e$, can be found as follows:

$$\left.\begin{aligned}
\frac{\partial U_{Pb}}{\partial x_{Wi}} &= \frac{4D_1 l_{P2}}{l_{P1}} \frac{1}{(1-f_{wPe})^2} \frac{\partial f_{wPe}}{\partial x_{Wi}} \\
\frac{\partial U_{Pb}}{\partial x_{Ni}} &= \frac{4D_2 l_{P1}}{l_{P2}} \frac{1}{(1-f_{nPs})^2} \frac{\partial f_{nPs}}{\partial x_{Ni}} \\
\frac{\partial U_{Pb}}{\partial x_{Pi}} &= \frac{4D_1 l_{P2}}{l_{P1}} \frac{1}{(1-f_{wPe})^2} \frac{\partial f_{wPe}}{\partial x_{Pi}} \\
&\quad + \frac{4D_2 l_{P1}}{l_{P2}} \frac{1}{(1-f_{nPs})^2} \frac{\partial f_{nPs}}{\partial x_{Pi}} \\
\frac{\partial U_{Pb}}{\partial x_{Si}} &= \frac{4D_2 l_{P1}}{l_{P2}} \frac{1}{(1-f_{nPs})^2} \frac{\partial f_{nPs}}{\partial x_{Si}} \\
\frac{\partial U_{Pb}}{\partial x_{Ei}} &= \frac{4D_1 l_{P2}}{l_{P1}} \frac{1}{(1-f_{wPe})^2} \frac{\partial f_{wPe}}{\partial x_{Ei}}
\end{aligned}\right\} \qquad [9.24]$$

and

$$\left.\begin{aligned}
\frac{\partial U_{bPa}}{\partial x_{Ai}} &= \left(E_1 \varepsilon_{Pa} \frac{\partial \varepsilon_{Pa}}{\partial x_{Ai}} + E_{12} \varepsilon_{Pb} \frac{\partial \varepsilon_{Pa}}{\partial x_{Ai}} + G\gamma_{bPa} \frac{\partial \gamma_{bPa}}{\partial x_{Ai}} \right) \cdot A_{bPa} \\
\frac{\partial U_{bPa}}{\partial x_{Pi}} &= \left(E_1 \varepsilon_{Pa} \frac{\partial \varepsilon_{Pa}}{\partial x_{Pi}} + E_2 \varepsilon_{Pb} \frac{\partial \varepsilon_{Pb}}{\partial x_{Pi}} + E_{12} \varepsilon_{Pa} \frac{\partial \varepsilon_{Pb}}{\partial x_{Pi}} \right. \\
&\quad \left. + E_{12} \varepsilon_{Pb} \frac{\partial \varepsilon_{Pa}}{\partial x_{Pi}} + G\gamma_{bPa} \frac{\partial \gamma_{bPa}}{\partial x_{Pi}} \right) \cdot A_{bPa} \\
\frac{\partial U_{bPa}}{\partial x_{Bi}} &= \left(E_2 \varepsilon_{Pb} \frac{\partial \varepsilon_{Pb}}{\partial x_{Bi}} + E_{12} \varepsilon_{Pa} \frac{\partial \varepsilon_{Pb}}{\partial x_{Bi}} + G\gamma_{bPa} \frac{\partial \gamma_{bPa}}{\partial x_{Bi}} \right) \cdot A_{bPa} \\
&(bPa = nPw, nPe, sPw, sPe)
\end{aligned}\right\} \qquad [9.25]$$

where

$$\frac{\partial \gamma_{bPa}}{\partial x_j} = -\frac{\partial \varphi_{bPa}}{\partial x_j} = \frac{1}{\sqrt{1-f_{bPa}^2}} \frac{\partial f_{bPa}}{\partial x_j}, \qquad (x_j = x_{Ai}, x_{Pi}, x_{Bi}, i = 1, 2, 3) \qquad [9.26]$$

For simplicity, in deriving equation 9.26, the coupling of bending in the two directions due to the Poisson's effect has been neglected (i.e. $D_{12} = 0$) and $A_P = l_{P1} l_{P2}$ has been used. There is currently little information on the Poisson's ratio of fabrics and its accurate measurement is difficult (Chen and Govindaraj, 1996). The effect of the Poisson's ratio is therefore ignored in almost all models belonging to the second approach. In finite-element shell models, while a non-zero Poisson's ratio can be easily handled and is quite often

included in numerical simulations, it has also been set to zero (Kim, 1991; Eischen *et al.*, 1996), a very small value (Kang and Yu, 1995) or not at all mentioned in the material properties (Gan *et al.*, 1995).

Collier (1991) compared the drape deformations of a circular piece of cloth draped over a circular pedestal using two very different values for the Poisson's ratios, 0.12 and 0.54 respectively, and showed that they led to some significant differences in the draped shape. A recent study by Chen and Govindaraj (1996) has, however, shown that the Poisson's ratio has no visible effect on fabric drape deformations for values between 0 and 0.5. Chen and Govindaraj (1996) also argued that Collier *et al.*'s results are not reliable due to the particular modelling approach used for their circular cloth pieces. It is also a pity that they did not include results for a Poisson's ratio of 0.3 which was used for other examples in their papers.

Even in the above two studies which give special attention to the effect of the Poisson's ratio, the definition of the Poisson's ratios is a little loose. Collier *et al.* does not even mention which of the two Poisson's ratios he was referring to when quoting the values, while Chen and Govindaraj define only one Poisson's ratio although the symmetry of the constitutive matrix is enforced. It thus appears to be wise to set the Poisson's ratios to zero. The theory presented here is, however, not limited to the case of zero Poisson's ratios, although a more involved derivation is required if a non-zero value is used. Numerical results given later in the section further justify the omission of the Poisson's effect.

In equations 9.24–9.26, the first derivatives of ε_{Pa} ($Pa = Pw, Pe, Pn, Ps$) and f_{bPa} ($bPa = wPe, nPs, nPw, nPe, sPw, sPe$) with respect to the nodal co-ordinates are given in the following four expressions

$$\left.\begin{aligned}\frac{\partial \varepsilon_{Pa}}{\partial x_{Pi}} &= \frac{x_{Pi} - x_{Ai}}{l_{PA} d_{PA}} \\ \frac{\partial \varepsilon_{Pa}}{\partial x_{Ai}} &= \frac{x_{Ai} - x_{Pi}}{l_{PA} d_{PA}}\end{aligned}\right\} (Pa = Pw, Pe, Pn, Ps; PA = PW, PE, PN, PS) \quad [9.27]$$

$$\left.\begin{aligned}\frac{\partial f_{bPa}}{\partial x_{Pi}} &= \frac{(2x_{Pi} - x_{Ai} - x_{Bi}) g_{bPa} - h_{bPa} \dfrac{\partial g_{bPa}}{\partial x_{Pi}}}{g_{bPa}^2} \\ \frac{\partial g_{bPa}}{\partial x_{Pi}} &= \frac{(x_{Pi} - x_{Ai}) d_{PB}}{d_{PA}} + \frac{(x_{Pi} - x_{Bi}) d_{PA}}{d_{PB}}\end{aligned}\right\} \quad [9.28]$$

$$\left.\begin{aligned}\frac{\partial f_{bPa}}{\partial x_{Ai}} &= \frac{x_{Bi} - x_{Pi}}{g_{bPa}} - \frac{h_{bPa}}{g_{bPa}^2} \frac{\partial g_{bPa}}{\partial x_{Ai}} \\ \frac{\partial g_{bPa}}{\partial x_{Ai}} &= \frac{(x_{Ai} - x_{Pi}) d_{PB}}{d_{PA}}\end{aligned}\right\} \quad [9.29]$$

and

$$\left.\begin{aligned}\frac{\partial f_{bPa}}{\partial x_{Bi}} &= \frac{x_{Ai} - x_{Pi}}{g_{bPa}} - \frac{h_{bPa}}{g_{bPa}^2}\frac{\partial g_{bPa}}{\partial x_{Bi}} \\ \frac{\partial g_{bPa}}{\partial x_{Bi}} &= \frac{(x_{Bi} - x_{Pi})d_{PA}}{d_{PB}}\end{aligned}\right\} \qquad [9.30]$$

By now, all components of the element internal force vector $\boldsymbol{F}^{\mathrm{e}}$ have been expressed as functions of the element nodal coordinate vector $\boldsymbol{X}^{\mathrm{e}}$. The global internal force vector $\boldsymbol{F}$ can then be formed by placing these components at appropriate positions according to the global grid-node numbering sequence.

9.2.4.2 The element tangent stiffness matrix

The element tangent stiffness matrix $\boldsymbol{K}^{\mathrm{e}}$ is a 15×15 symmetric matrix. For the typical internal control volume P, the matrix is

$$\boldsymbol{K}^{\mathrm{e}} = \begin{bmatrix} \dfrac{\partial^2 U_P}{\partial x_{Wi}\partial x_{Wk}} & & & & \\ \dfrac{\partial^2 U_P}{\partial x_{Ni}\partial x_{Wk}} & \dfrac{\partial^2 U_P}{\partial x_{Ni}\partial x_{Nk}} & & \textit{Sym.} & \\ \dfrac{\partial^2 U_P}{\partial x_{Pi}\partial x_{Wk}} & \dfrac{\partial^2 U_P}{\partial x_{Pi}\partial x_{Nk}} & \dfrac{\partial^2 U_P}{\partial x_{Pi}\partial x_{Pk}} & & \\ \dfrac{\partial^2 U_P}{\partial x_{Si}\partial x_{Wk}} & \dfrac{\partial^2 U_P}{\partial x_{Si}\partial x_{Nk}} & \dfrac{\partial^2 U_P}{\partial x_{Si}\partial x_{Pk}} & \dfrac{\partial^2 U_P}{\partial x_{Si}\partial x_{Sk}} & \\ \dfrac{\partial^2 U_P}{\partial x_{Ei}\partial x_{Wk}} & \dfrac{\partial^2 U_P}{\partial x_{Ei}\partial x_{Nk}} & \dfrac{\partial^2 U_P}{\partial x_{Ei}\partial x_{Pk}} & \dfrac{\partial^2 U_P}{\partial x_{Ei}\partial x_{Sk}} & \dfrac{\partial^2 U_P}{\partial x_{Ei}\partial x_{Ek}} \end{bmatrix} \qquad [9.31]$$

in which each component stands for a 3×3 sub-matrix. For example

$$\left[\frac{\partial^2 U_P}{\partial x_{Ni}\partial x_{Wk}}\right] = \begin{bmatrix} \dfrac{\partial^2 U_P}{\partial x_{N1}\partial x_{W1}} & \dfrac{\partial^2 U_P}{\partial x_{N1}\partial x_{W2}} & \dfrac{\partial^2 U_P}{\partial x_{N1}\partial x_{W3}} \\ \dfrac{\partial^2 U_P}{\partial x_{N2}\partial x_{W1}} & \dfrac{\partial^2 U_P}{\partial x_{N2}\partial x_{W2}} & \dfrac{\partial^2 U_P}{\partial x_{N2}\partial x_{W3}} \\ \dfrac{\partial^2 U_P}{\partial x_{N3}\partial x_{W1}} & \dfrac{\partial^2 U_P}{\partial x_{N3}\partial x_{W2}} & \dfrac{\partial^2 U_P}{\partial x_{N3}\partial x_{W3}} \end{bmatrix} \qquad [9.32]$$

Using equations 9.17 and 9.18, the second partial derivatives may be expressed as

$$\left.\begin{aligned}
&\frac{\partial^2 U_P}{\partial x_j \partial x_l} = \frac{\partial^2 U_{Pb}}{\partial x_j \partial x_l} + \frac{\partial^2 U_{Pm}}{\partial x_j \partial x_l} \\
&\frac{\partial^2 U_{Pm}}{\partial x_j \partial x_l} = \frac{\partial^2 U_{nPw}}{\partial x_j \partial x_l} + \frac{\partial^2 U_{nPe}}{\partial x_j \partial x_l} + \frac{\partial^2 U_{sPw}}{\partial x_j \partial x_l} + \frac{\partial^2 U_{sPe}}{\partial x_j \partial x_l} \\
&(x_j, x_l = x_{Wi}, x_{Ni}, x_{Pi}, x_{Si}, x_{Ei}, i = 1, 2, 3)
\end{aligned}\right\} \quad [9.33]$$

The second partial derivatives of the bending strain energy U_{Pb} can be obtained by differentiating equation 9.24 with respect to nodal co-ordinates once more, which leads to

$$\begin{aligned}
&\frac{\partial^2 U_{Pb}}{\partial x_{Pi} \partial x_{Pk}} \\
&= \frac{4 D_1 l_{P2}}{l_{P1}} \left[\frac{1}{(1 - f_{wPe})^2} \frac{\partial^2 f_{wPe}}{\partial x_{Pi} \partial x_{Pk}} + \frac{2}{(1 - f_{wPe})^3} \frac{\partial f_{wPe}}{\partial x_{Pi}} \frac{\partial f_{wPe}}{\partial x_{Pk}} \right] \\
&+ \frac{4 D_2 l_{P1}}{l_{P2}} \left[\frac{1}{(1 - f_{nPs})^2} \frac{\partial^2 f_{nPs}}{\partial x_{Pi} \partial x_{Pk}} + \frac{2}{(1 - f_{nPs})^3} \frac{\partial f_{nPs}}{\partial x_{Pi}} \frac{\partial f_{nPs}}{\partial x_{Pk}} \right]
\end{aligned} \quad [9.34]$$

and

$$\begin{aligned}
&\frac{\partial^2 U_{Pb}}{\partial x_{Wi} \partial x_{Wk}} \\
&= \frac{4 D_1 l_{P2}}{l_{P1}} \left[\frac{1}{(1 - f_{wPe})^2} \frac{\partial^2 f_{wPe}}{\partial x_{wi} \partial x_{Wk}} + \frac{2}{(1 - f_{wPe})^3} \frac{\partial f_{wPe}}{\partial x_{Wi}} \frac{\partial f_{wPe}}{\partial x_{Wk}} \right]
\end{aligned} \quad [9.35]$$

The other four terms $\partial^2 U_{Pb}/\partial x_{Pi} \partial x_{Wk}$, $\partial^2 U_{Pb}/\partial x_{Ei} \partial x_{Wk}$, $\partial^2 U_{Pb}/\partial x_{Ei} \partial x_{Pk}$ and $\partial^2 U_{Pb}/\partial x_{Ei} \partial x_{Ek}$ can be found by appropriate permutations in the subscripts of the nodal co-ordinates on both sides of equation 9.35. Similarly,

$$\begin{aligned}
&\frac{\partial^2 U_{Pb}}{\partial x_{Ni} \partial x_{Ni}} \\
&= \frac{4 D_2 l_{P1}}{l_{P2}} \left[\frac{1}{(1 - f_{nPs})^2} \frac{\partial^2 f_{nPs}}{\partial x_{Ni} \partial x_{Nk}} + \frac{2}{(1 - f_{nPs})^3} \frac{\partial f_{nPs}}{\partial x_{Ni}} \frac{\partial f_{nPs}}{\partial x_{Nk}} \right]
\end{aligned} \quad [9.36]$$

Again, the terms $\partial^2 U_{Pb}/\partial x_{Pi} \partial x_{Nk}$, $\partial^2 U_{Pb}/\partial x_{Si} \partial x_{Nk}$, $\partial^2 U_{Pb}/\partial x_{Si} \partial x_{Pk}$ and $\partial^2 U_{Pb}/\partial x_{Si} \partial x_{Sk}$ can be obtained by permutations in the subscripts on both sides of equation 9.36. The second derivatives of f_{bPa} ($bPa = wPs$, nPs, nPw, nPe, sPw, sPe) can be derived without difficulty. The second derivatives of the in-plane strain energy function U_{bPa} ($bPa = nPw$, nPe, sPw, sPe) can also be

obtained by differentiating equation 9.25 once more with respect to the nodal co-ordinates.

9.2.5 Boundary control volumes

In the previous sections, the element internal force vector $\boldsymbol{F}^{\mathrm{e}}$ and the element tangent stiffness matrix $\boldsymbol{K}^{\mathrm{e}}$ for internal control volumes are established. The corresponding matrices for boundary control volumes, such as the edge volume P_1 and the corner volume P_2 as shown in Fig. 9.1, are now derived. For an edge control volume such as the typical volume P_1 in Fig. 9.1, the strain energy U_{P1} only depends on four grid nodes. Therefore, the element internal force vector $\boldsymbol{F}^{\mathrm{e}}$ is a 12×1 vector and the element tangent stiffness matrix $\boldsymbol{K}^{\mathrm{e}}$ is a 12×12 matrix. They are expressed as follows

$$\boldsymbol{F}^{\mathrm{e}} = \left[\frac{\partial U_P}{\partial x_{Ni}} \; \frac{\partial U_P}{\partial x_{Pi}} \; \frac{\partial U_P}{\partial x_{Si}} \; \frac{\partial U_P}{\partial x_{Ei}} \right]^{\mathrm{T}} \qquad [9.37]$$

and

$$\boldsymbol{K}^{\mathrm{e}} = \begin{bmatrix} \dfrac{\partial^2 U_P}{\partial x_{Ni}\partial x_{Nk}} & & & \textit{Sym.} \\ \dfrac{\partial^2 U_P}{\partial x_{Pi}\partial x_{Nk}} & \dfrac{\partial^2 U_P}{\partial x_{Pi}\partial x_{Pk}} & & \\ \dfrac{\partial^2 U_P}{\partial x_{Si}\partial x_{Nk}} & \dfrac{\partial^2 U_P}{\partial x_{Si}\partial x_{Pk}} & \dfrac{\partial^2 U_P}{\partial x_{Si}\partial x_{Sk}} & \\ \dfrac{\partial^2 U_P}{\partial x_{Ei}\partial x_{Nk}} & \dfrac{\partial^2 U_P}{\partial x_{Ei}\partial x_{Pk}} & \dfrac{\partial^2 U_P}{\partial x_{Ei}\partial x_{Sk}} & \dfrac{\partial^2 U_P}{\partial x_{Ei}\partial x_{Ek}} \end{bmatrix} \qquad [9.38]$$

Similarly, for a corner control volume, such as the typical volume P_2 shown in Fig. 9.1, the strain energy U_{P2} depends only on three grid nodes, so $\boldsymbol{F}^{\mathrm{e}}$ is a 9×1 vector and $\boldsymbol{K}^{\mathrm{e}}$ a 9×9 matrix. These are given by

$$\boldsymbol{F}^{\mathrm{e}} = \left[\frac{\partial U_P}{\partial x_{Ni}} \; \frac{\partial U_P}{\partial x_{Pi}} \; \frac{\partial U_P}{\partial x_{Ei}} \right]^{\mathrm{T}} \qquad [9.39]$$

and

$$\boldsymbol{K}^{\mathrm{e}} = \begin{bmatrix} \dfrac{\partial^2 U_P}{\partial x_{Ni}\partial x_{Nk}} & & \textit{Sym.} \\ \dfrac{\partial^2 U_P}{\partial x_{Pi}\partial x_{Nk}} & \dfrac{\partial^2 U_P}{\partial x_{Pi}\partial x_{Pk}} & \\ \dfrac{\partial^2 U_P}{\partial x_{Ei}\partial x_{Nk}} & \dfrac{\partial^2 U_P}{\partial x_{Ei}\partial x_{Pk}} & \dfrac{\partial^2 U_P}{\partial x_{Ei}\partial x_{Ek}} \end{bmatrix} \qquad [9.40]$$

The procedure of derivation for all components in equations 9.37–9.40 is the same as that for internal control volumes as presented in the previous sections.

9.2.6 Solution method for the non-linear equations

9.2.6.1 Existing solution procedures in fabric deformation analysis

A variety of algorithms have been employed for the solution of the non-linear algebraic equations arising from a discretised fabric model. In Breen *et al*.'s work (Breen, 1993; Breen *et al*., 1994) the deformed shapes of square pieces of woven cloth draped over rectangular tables were simulated using a particle-system model. They used a three-phase solution procedure. The first phase accounts for the effect of gravity and the collisions between the cloth and the interacting object. The second phase is an energy minimisation phase in which a stochastic technique is used to reach a local minimum. In the third phase, a stochastic perturbation technique is used to produce a more natural final shape.

Eberhardt *et al*. (1996) used a Runge-Kutta method with adaptive step-size control and the Bulirsch-Stoer method (Press *et al*., 1992) as a numerical solver for the differential equations resulting from the particle-system model. The simulation examples presented include cloth sheets draped over a square table, a circular table and a sphere. Other researchers (Kim, 1991; Chen and Govindaraj, 1995; Gan *et al*., 1995; Kang and Yu, 1995) employed the incremental Newton–Raphson iteration method to solve the non-linear equilibrium equations derived from a finite-element formulation. Their simulation examples include the two-dimensional draping of fabric cantilevers, square cloth sheets draped over cubic objects or circular tables. Deng (1994) and Eischen *et al*. (1996) employed an adaptive arc-length algorithm (Riks, 1979; Schweizerhof and Wriggers, 1986) with an acceleration factor to deal with non-linear effects including material non-linearity and contact. The predicted results of fabric pieces draped over a block, hanging over a round rod, draped over intersecting cylinders were presented.

In the existing literature, little discussion has been found on an appropriate solution procedure for fabric deformation analysis which takes into account the special characteristics of these problems. This issue is considered first below, leading to the choice of the Newton–Raphson method (Crisfield, 1991; Bathe, 1996) in conjunction with the use of the line search technique (Crisfield, 1991). The effectiveness and efficiency of the solution procedure is then investigated, through comparison with the conventional step-by-step incremental iterative Newton–Raphson procedure in a numerical example.

9.2.6.2 Special characteristics of fabric deformation analysis

Fabric deformations generally involve very large displacements, often of the order of hundreds of times the thickness of the fabric sheet. This kind of gross deformation is not encountered in the analysis of load-bearing structures. The only obvious example in non-linear structural mechanics which is closely related to this class of deformations is the elastica problem. There are also some other major differences between a fabric drape deformation analysis and a non-linear analysis of load-bearing structures. First, the aim of a fabric deformation analysis is to determine the final deformed shape under self weight with or without additional applied loading, while in the non-linear analysis of load-bearing structures, the maximum load-carrying capacity and the load-deflection response are of interest. Second, both the displacements and the internal forces need to be carefully determined in the analysis of load-bearing structures, while in a fabric deformation analysis, the final displacements are the only item of interest.

It is easy to see that a step-by-step incremental iterative approach is well suited for the analysis of load-bearing structures, as the load-deflection response can be traced and internal forces and displacements can be computed at different levels of loading. For a fabric deformation analysis, a more direct and efficient approach is clearly desirable as the only information of interest is the final displacements of the cloth sheet.

9.2.6.3 The Newton–Raphson method

Based on the above rationale, the full Newton–Raphson iterative method (Crisfield, 1991; Bathe, 1996) is adopted for the solution of the non-linear equations of the fabric sheet with all the loading applied in a single step, instead of an incremental iterative approach. The solution process using the Newton–Raphson iterative method (Crisfield, 1991; Bathe, 1996) in a single step is described by the following two equations

$$\left.\begin{aligned} \boldsymbol{K}\Delta\boldsymbol{X} &= \boldsymbol{R} - \boldsymbol{F} \\ \boldsymbol{X}^{\text{new}} &= \boldsymbol{X}^{\text{old}} + \Delta\boldsymbol{X} \end{aligned}\right\} \qquad [9.41]$$

where $\boldsymbol{X}$ is the global nodal co-ordinate vector, $\boldsymbol{K}$ is the global tangent stiffness matrix, $\boldsymbol{F}$ is the global nodal internal force vector and $\boldsymbol{R}$ is the global nodal load vector due to gravity and other applied loads if any. Details of the computational steps will be given later.

9.2.6.4 The line search technique

To accelerate the convergence of the Newton–Raphson iterative solution process, the line search technique (Crisfield, 1991) is included in the iterative

solution process. In this technique, the incremental co-ordinate vector $\Delta \boldsymbol{X}$ obtained from the first part of equation 9.41 is now defined as an iterative direction for the actual co-ordinate increment. The co-ordinate vector is then updated using

$$\boldsymbol{X}^{\text{update}} = \boldsymbol{X}^{\text{old}} + \eta \Delta \boldsymbol{X} \qquad [9.42]$$

in which the scalar η is the iterative step length and the only variable for the line-search process. The scalar η can be determined using the linear interpolation method until the defined inner product

$$s(\eta) = \Delta \boldsymbol{X}^{\text{T}}(\boldsymbol{F} - \boldsymbol{R}) \qquad [9.43]$$

is small, i.e. until the following expression is satisfied

$$|s(\eta)| < \beta_{\text{ls}} |s(\eta = 0)| \qquad [9.44]$$

where β_{ls} is the line-search tolerance. In the numerical simulations to be presented later, the line-search technique was employed in the solution process for all-three dimensional cases and was found to be effective. For the two-dimensional draping analysis of fabric cantilevers, this technique was not used as it was not found to be useful.

9.2.6.5 Convergence criterion

A rational and realistic convergence criterion is an essential ingredient of an effective iterative solution procedure. As stated by Bathe (1996), 'if the convergence tolerances are too loose, inaccurate results are obtained, and if the tolerances are too tight, much computational effort is spent to obtain needless accuracy'. A number of convergence criteria have been used in non-linear analysis of load-bearing structures (Bathe, 1996), which may be either displacement-based or load-based. Bearing in mind that the concern in fabric drape deformation analysis is the final deformed shape, the convergence criterion adopted is the iterative change of the position vector at a grid node which is given by

$$\left.\begin{aligned} \beta &= \frac{|\Delta^{\text{new}} - \Delta^{\text{old}}|}{\Delta^{\text{new}}} \leq \beta_{\text{d}} \\ \Delta^{\text{new}} &= (\sqrt{x^2 + y^2 + z^2})^{\text{new}}, \Delta^{\text{old}} = (\sqrt{x^2 + y^2 + z^2})^{\text{old}} \end{aligned}\right\} \qquad [9.45]$$

where β_{d} is the displacement convergence tolerance, x, y and z are the three co-ordinates of the grid node. This criterion has to be satisfied by each grid node before convergence is deemed to have been reached. A value of 10^{-5} has been used and found to be satisfactory in all the numerical simulations presented below.

9.3 References

Ascough J, Bez H E and Bricis A M (1996), A simple finite element model for cloth drape simulation, *Int J Clothing Sci and Tech*, **8**(3), 59–74.

Bailey C and Cross M (1995), A finite volume procedure to solve elastic solid mechanics problems in three dimensions on an unstructured mesh, *Int J Numer Methods Eng*, **38**, 1757–1776.

Bathe K J (1982), *Finite Element Procedures in Engineering Analysis*, New Jersey, Prentice Hall.

Bathe K J (1996), *Finite Element Procedures*, New Jersey, Prentice Hall.

Breen D E (1993), *A Particle-based Model for Simulating the Draping Behaviour of Woven Cloth* (Doctoral dissertation, Rensselaer Polytechnic Inst., New York).

Breen D E, House D H and Getto P H (1991), A particle-based computational model of cloth draping behaviour, in *Scientific Visualization of Physical Phenomena*, Patrikalakis N M (ed), New York, Springer Verlag, 113–134.

Breen D E, House D H and Getto P H (1992), A particle-based particle model of woven cloth, *The Visual Computer*, **8**(5–6), 264–277.

Breen D E, House D H and Wozny M J (1994), A particle-based model for simulating the draping behaviour of woven cloth, *Text. Res J*, **64**(11), 663–685.

Carignan M, Yang Y, Thalmann N M and Thalmann D (1992), Dressing animated synthetic actors with complex deformable clothes, *Computer Graphics* (*Proc. siggraph)*, **26**(2), 99–104.

Chen B and Govindaraj M (1995), A physical based model of fabric drape using flexible shell theory, *Text Res J*, **65**(6), 324–330.

Chen B and Govindaraj M (1996), A parametric study of fabric drape, *Text Res J*, **66**(1), 17–24.

Collier B J (1991), Measurement of fabric drape and its relation to fabric mechanical properties and subjective evaluation, *Clothing & Text Res J*, **10**(1), 46–52.

Crisfield M A (1991), *Non-linear Finite Element Analysis of Solids and Structures, vol.1: Essentials*, Chichester, John Wiley & Sons.

Demirdzic I and Martinovic D (1993), Finite volume method for thermo-elasto-plastic stress analysis, *Comput Methods Appl Mech Eng*, **109**, 331–349.

Demirdzic I and Muzaferija S (1994), Finite volume method for stress analysis in complex domain, *Int J Numer Methods Eng*, **37**, 3751–3766.

Deng S (1994), *Nonlinear Fabric Mechanics Including Material Nonlinearity, Contact, and an Adaptive Global Solution Algorithm* Doctoral Dissertation, (North Carolina State University, Raleigh NC).

Dhande S G, Rao P V M and Moore C L (1993), Geometric modelling of draped fabric surfaces, *Graphics, design and visualization (Proc Int Conf on Computer Graphics)*, Mudur S P and Pattanaik S N (eds), Bombay, Jaico Publishing House, 173–180.

Eberhardt B, Weber A and Strasser W (1996), A fast, flexible particle-system model for cloth draping, *IEEE Computer Graphics and Applications*, **16**(5), 51–59.

Eischen J W, Deng S and Clapp T G (1996), Finite-element modelling and control of flexible fabric parts, *IEEE Computer Graphics and Applications*, **16**(5), 71–80.

Feynman C (1986), *Modelling the Appearance of Cloth*, Master's dissertation, Massachusetts Institute of Technology, Cambridge).

Fryer Y D, Bailey C, Cross M and Lai C H (1991), A control volume procedure for solving the elastic stress-strain equations on an unstructured mesh, *Appl Math Modelling*, **15**(11–12), 639–645.

Gan L, Ly N G and Steven G P (1995), A study of fabric deformation using nonlinear finite elements, *Text Res J*, **65**(11), 660–668.

Hu J L and Teng J G (1996), 'Computational fabric mechanics-present status and future trends', *Finite Element in Analysis and Design*, **21**, 225–237.

Kang T J and Yu W R (1995), Drape simulation of woven fabric by using the finite-element method, *J Text Inst*, **86**(4), 635–648.

Kawabata S (1975), *The Standardization and Analysis of Hand Evaluation*, Osaka, Hand evaluation and standardization committee of the Textile Machinery Society of Japan.

Kim J (1991), *Fabric Mechanics Analysis Using Large Deformation Orthotropic Shell Theory*, Doctoral Dissertation, North Carolina State University, Raleigh, N C).

Lloyd D W (1980), The analysis of complex fabric deformations, in *Mechanics of Flexible Fibre Assemblies (NATO Advanced Study Institute Series; E Appplied Sciences No. 38*), Hearle J W S, Thwaites J J and Amirbayat J (eds), The Netherlands Alpen aan den Rijn, Sijthoff & Noordhoff, 311–342.

Ng H N and Grimsdale R L (1996), Computer graphics techniques for modelling cloth, *IEEE Computer Graphics and Applications*, **16**, 28–41.

Onate E, Cervera M and Zienkiewicz O C (1994), Finite volume format for structural mechanics, *Int J Numer Methods Eng*, **37**(2), 181–201.

Patankar S V (1980), *Numerical Heat Transfer and Fluid Flow*, New York, Hemisphere Publishing Corporation.

Press W H, Flannery B P, Teukolsky S A and Vetterling W T (1992), *Numerical Recipes in C: The Art of Scientific Computing, 2nd edition*, New York, Cambridge University Press.

Riks E (1979), An acceleration approach to the solution of snapping and buckling problem, *Int J Solids Struc*, **15**, 524–551.

Schnobrich W C and Pecknold D A (1973), The lumped-parameter or bar-node model approach to thin shell analysis, numerical and computer methods, in *Structural Mechanics*, Perrone F and Schnobrich R (eds), London, Academic Press, 337–402.

Schweizerhof K H and Wriggers P (1986), Consistent linearization of path following methods in nonlinear FE analysis, *Comput Methods Appl Mech Eng*, **72**, 267–304.

Simo J C and Fox D D (1989), On a stress resultant geometrically exact shell model part I: formulation and parameterization, *Comp Methods Appl Mech Eng*, **72**, 267–304.

Simo J C and Fox D D and Rifai M S (1989), On a stress resultant geometrically exact shell model part II: the linear theory; computational aspects, *Comp Methods Appl Mech Eng*, **73**, 53–92.

Simo J C, Fox D D and Rifai M S (1990), On a stress resultant geometrically exact shell model, Part III, Aspects of nonlinear theory, *Comp Methods Appl Mech Eng*, **79**, 21–70.

Stylios G K, Wan T R and Powell N J (1995), Modelling the dynamic drape of fabrics on synthetic humans, a physical, lumped-parameter model, *Int J Clothing Sci and Tech*, **7**(5), 10–25.

Stylios G K, Wan T R and Powell N J (1996), Modelling the dynamic drape of garments on synthetic humans in a virtual fashion show, *Int J Clothing Sci and Tech*, **8**(3), 95–112.

Terzopoulos D, Platt J, Barr A and Fleischer K (1987), Elastically deformable models, *Computer Graphics*, **21**(4), 205–214.

Thalmann N M and Thalmann D (1991), Cloth animation with self-collision detection, in *Modelling in Computer Graphics*, Kunii T L (ed), Berlin, Springer-Verlag, 179–187.

Thalmann N M and Yang Y (1991), Techniques for cloth animation, in *New Trends in Animation and Visualization*, Thalmann N M and Thalmann D (eds), Chichester, John Wiley & Sons, 243–256.

Versteeg H K and Malalasekera W (1995), *An Introduction to Computational Fluid Dynamics, the Finite Volume Method*, Harlow, Longman Scientific & Technical.

Weil J (1986), The synthesis of cloth object, *Computer Graphics (Proc Siggraph)*, **20**(4), 49–54.

Wheel M A (1996), Finite volume approach to the stress analysis of pressurized axisymmetric structures, *Int J Pressure Vessels Piping*, **68**(3), 311–317.

Wheel M A (1997), A finite volume method for analyzing the bending deformation of thick and thin plates, *Comp Methods Appl Mech Eng*, **147**, 199–208.

Yu W R, Kang T J and Lee J K (1993), Drape properties of woven fabrics, *Proc 2nd Asian Textile Conf*, **1**, South Korea, 20 Oct, 455–459.